Design Concept to Reduce Fuel NO_x in Catalytic Combustion of Gasified Biomass

Johan C. G. Andrae and Pehr H. Björnbom
Dept. of Chemical Engineering and Technology, Royal Institute of Technology, SE-100 44 Stockholm, Sweden

Peter Glarborg
Dept. of Chemical Engineering, Technical University of Denmark, DK-2800 Lyngby, Denmark

A reactor concept was studied to reduce the fuel NO_x at conditions relevant to catalytic combustion of gasified biomass containing ammonia. A hybrid reactor is modeled with passive and active channels, where only part of the fuel is combusted catalytically in the active channels. The completion of the reactions is carried out in the subsequent homogeneous zone. The air − fuel ratio is found to be the most important parameter for the NO_x emission level. When the primary zone is operated fuel-lean, no favorable conditions are established for selective noncatalytic reduction reactions in the homogeneous zone, and the fuel nitrogen is largely oxidized to NO. However, if the air supply to the monolith is staged rich-lean, a 95% reduction in NO is possible. The NO reduction is facilitated by the remaining fuel components, CO and H_2.

Introduction

As a result of the growing concern for the effects of increasing emissions of CO_2 caused by the extensive use of fossil fuels, the use of biomass for power production is becoming more important. One possibility is to use gasified biomass in gas turbines. Compared to natural gas, the fuels from gasification of biomasses are quite complex mixtures, consisting of CO, H_2, CH_4, and to a minor extent C_2H_4 as combustible components along with gasification byproducts, CO_2 and H_2O, and N_2. Also present are minor amounts of N- and S-containing compounds, tars, and aerosols. For example, biogas contains NH_3, H_2S, and alkali compounds. Ammonia may be oxidized to nitrogen oxides, leading to increased NO_x emissions, and the sulfur gives rise to SO_2 during the combustion. The use of gasified biomass is often considered for scales and/or locations where ultralow NO_x emissions are not required. However, it is reasonable to expect that future emission standards for NO_x will be more stringent even for these applications.

Some of the available techniques to control NO_x emissions from heavy-duty industrial gas turbines are diluents injection in the combustor reaction zone, and lean premixed dry low NO_x (DLN) combustion. For ultralow emissions requirements, these must be combined with selective catalytic reduction (SCR) De-$NO_{(x)}$ systems in the gas turbine exhaust. Also high-temperature catalytic combustion for gas-turbine applications has been investigated in recent years because of its potential to minimize NO_x, unburned hydrocarbons. and CO emissions (for example, Johansson et al., 1999; Forzatti and Groppi, 1999; Groppi et al., 2000). While catalytic combustion of natural gas has been developed for the purpose of ultralow emission of NO_x, the catalytic combustion of gasified biomass may have other motives. Gasified biomass is a low-heating-value gas, and catalytic combustion may be attractive compared to conventional combustion due to its higher combustion stability and safer ignition. However, special attention must be paid since sulfur and alkali compounds may be poisonous to the catalyst.

The considerable levels of NH_3 in the gasified biomass cause fuel-NO_x to be the dominant source of nitrogen oxides. Johansson (1998) and Burch and Southward (2000, 2001) reviewed previous work on fuel-NO_x reduction in catalytic combustion of gasified biomass. In an earlier work on fuel-NO_x abatement, Clark et al. (1982) performed a bench-scale testing of three pressurized combustion chambers: a catalytic combustor, a diffusion flame, and a perfectly stirred reactor. They used a synthetic low-heating-value gas simulating gasi-

Correspondence concerning this article should be addressed to J. C. G. Andrae.

fied coal with the addition of NH_3 to simulate fuel-N. The catalytic reactor converted 14% of the ammonia to NO_x, compared to 22–33% and 50% to NO_x for the diffusion flame and the perfectly stirred reactor, respectively. The lowest conversion of NH_3 to NO_x was achieved when the catalyst was staged fuel rich–fuel lean with reduction of NO_x in the fuel-rich region, and a $Pt/NiO/ZrO_2$-catalyst was superior compared to a Pt/Al_2O_3-catalyst. Recent work has mainly investigated the possibilities for selective oxidation of ammonia to nitrogen by the combustion catalyst. Lietti et al. (1999) studied Pd-based catalysts and attributed a fairly low NO_x reduction effect solely to reactions in the gas phase. The best results so far seem to be those of Burch and Southward (2001). They used fuel-rich catalytic combustion of biogas at atmospheric pressure and could obtain selective oxidation of ammonia to nitrogen over Rh and Ir catalysts for temperatures above 873 K (99.5% NO_x reduction). They attributed the NO_x reduction effect to reactions on the catalyst surface.

High-temperature catalytic combustion also has to deal with the problem of the instability of catalyst materials at high temperatures. This problem is discussed in several reviews on high-temperature catalytic combustion (for example, Johansson et al., 1999; Forzatti and Groppi, 1999). One important method to solve this problem is to use a combustion chamber with catalytic stages up to a limited temperature (for example, 1,000 K) followed by a homogeneous combustion zone without catalyst for the combustion up to the inlet temperature for the turbine (for example, 1,573 K, as used in this work). This is called a hybrid catalytic combustion chamber and avoids the necessity for very sophisticated catalyst materials for the catalytic segments (Groppi et al., 1995; Dalla Betta et al., 1995).

In this work we have for the first time to our knowledge, by using a mathematical simulation with detailed combustion kinetics, investigated the possibilities of obtaining fuel-NO_x reduction in hybrid combustion chambers fueled with biogas. We simulate a ceramic monolith where part of the fuel is combusted in active channels, followed by a homogeneous zone where the combustion is completed. Our main objective has been to search for favorable conditions for minimizing NO_x emissions from the hybrid combustion chamber. The approach is to use the potential reducing agents present in the gasified biomass to convert NO to N_2 in the homogeneous combustion section of the combustor. The reducing agents are NH_3, which may react with NO under conditions favorable for selective noncatalytic reduction (SNCR), or the fuel components, which may reduce NO in reburn-type reactions. We have investigated various designs and operational conditions of hybrid catalytic combustors for that purpose.

Numerical Model

The gas-turbine combustion chamber model is outlined in Figure 1. With the assumption that there is laminar flow, negligible heat dispersion, and uniform distribution of the gas properties at the inlet to the monolith, a single two-dimensional (2-D) channel has been modeled using the program CRESLAF (Coltrin et al., 1993), which is part of the CHEMKIN Collection (Kee et al., 2000). CRESLAF solves the boundary-layer equations, and a cylindrical channel is used here to approximate the actual shape of the channels.

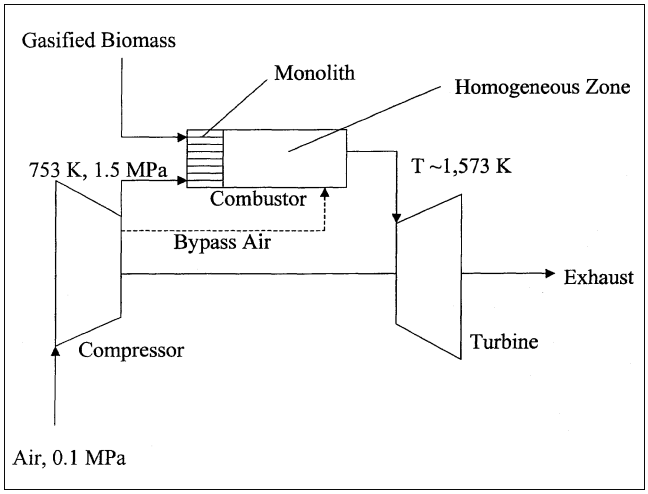

Figure 1. The gas-turbine combustion-chamber model.

The governing equations for a steady flow are

Mass continuity

$$\frac{\partial \rho u}{\partial z} + \frac{1}{r}\frac{\partial (r\rho v)}{\partial r} = 0 \tag{1}$$

Axial momentum

$$\rho u\frac{\partial u}{\partial z} + \rho v\frac{\partial u}{\partial r} + \frac{\partial p}{\partial z} - \frac{1}{r}\frac{\partial}{\partial r}\left(\mu r\frac{\partial u}{\partial r}\right) = 0 \tag{2}$$

Cross-flow momentum

$$\frac{\partial p}{\partial r} = 0 \tag{3}$$

Species continuity

$$\rho u\frac{\partial Y_j}{\partial z} + \rho v\frac{\partial Y_j}{\partial r} - \frac{1}{r}\frac{\partial r J_{j,r}}{\partial r} - \dot{\omega}_j W_j = 0 \qquad \left(j = 1,\ldots,K_g\right) \tag{4}$$

Energy

$$\rho c_p\left(u\frac{\partial T}{\partial z} + v\frac{\partial T}{\partial r}\right) - \frac{1}{r}\frac{\partial}{\partial r}\left(rk\frac{\partial T}{\partial r}\right) + \sum_{j=i}^{K_g} c_{p,j}J_{j,r}\frac{\partial T}{\partial r} + \sum_{j=1}^{K_g} h_j\dot{\omega}_j W_j = 0 \tag{5}$$

State

$$\rho = \frac{p}{RT}\frac{1}{\sum_{j=1}^{K_g} Y_j/W_j} \tag{6}$$

Due to computational advantages, in CRESLAF the boundary-layer equations are recast using the Von Mises transformation (see, for example, Kee et al., 2003). More-

over, the cylindrical channel is discretized into 30–60 radial mesh points from the centerline with the mesh points concentrated near the wall.

In Eqs. 4 and 5 the mass flux in the radial direction is given by

$$J_{j,r} = -\rho \frac{W_j}{\overline{W}} D_{j,m} \frac{\partial X_j}{\partial r} - D_j^T \frac{1}{T} \frac{\partial T}{\partial r} \tag{7}$$

Inlet conditions

Each individual channel in the monolith has the height of one millimeter. The pressure and velocity after the compressor is 1.5 MPa and 1.0 m/s, respectively, and air and fuel are mixed to different primary λ-values, where λ denotes the excess air ratio

$$\lambda = \frac{\text{actual air} - \text{fuel ratio}}{\text{stoichiometric air} - \text{fuel ratio}} \tag{8}$$

The inlet temperature to the monolith is 753 K, a typical inlet temperature for the catalytic section of hybrid combustors (Groppi et al., 1995). To obtain a final gas temperature to the turbine of ~1573 K, the overall excess air ratio is 2.5.

Boundary conditions

At the catalytic walls (active channels) the composition is described in terms of surface-species site fractions. The site fraction for species j is at every axial position determined by equations

$$\dot{s}_j = \sum_{i=1}^{N_s} \nu_{ij} r_i^s = 0 \qquad (j = 1, \ldots, K_s - 1) \tag{9}$$

$$\sum_{j=1}^{K_S} Z_j = 1 \tag{10}$$

For one surface species, the steady-state condition given by Eq. 9 is not solved, but instead Eq. 10 is used, which requires that the site fractions sum to unity.

The flux of gas-phase species j to the wall is balanced by surface production and destruction of the species by surface reactions

$$\dot{s}_j W_j = J_{j,r} + \rho Y_j \nu_{st} \qquad (j = 1, \ldots, K_g) \tag{11}$$

The Stefan velocity (ν_{st}) is the surface-normal fluid velocity that is associated with a net mass change at a reacting surface.

On the chemically inert walls (passive channels) a zero-gradient Neumann boundary condition is used for each species mass fraction

$$\left(\frac{\partial Y_j}{\partial r} \right)_{r=0} = 0 \qquad (j = 1, \ldots, K_g) \tag{12}$$

For an adiabatic wall, the boundary condition for the temperature is determined with an energy balance

$$k \left(\frac{\partial T}{\partial r} \right)_{r=0} + \sum_{j=1}^{K_g} J_{j,r} h_j - \sum_{j=1}^{K_s} \dot{s}_j W_j h_j = 0 \tag{13}$$

For the nonadiabatic wall, the boundary condition for the surface temperature is $T = T_s$. Moreover, the axial velocity is assumed to be zero at the wall (the nonslip condition). Symmetry is used to specify the boundary conditions at the channel center line in the axisymmetric channel. In a hybrid catalytic combustor, the configuration with active and passive channels results in heat transfer from the active channels to the nonactive channels, thereby significantly lowering the exit temperature from the monolith compared to an adiabatic channel (Groppi et al., 1995; Dalla Betta et al., 1995). The approach adopted here to estimate the axial temperature profile of the catalyst surface is to first assume an adiabatic channel, that is, without any cooling from adjacent passive channels. Then the surface temperature profile is reevaluated assuming that the actual temperature rise with respect to the gas inlet temperature is a fraction of the adiabatic temperature rise equal to the fraction of active channels. We assume that there is temperature equilibrium between the active and passive channels, and that the temperature rise and conversion is proportional according to the equation

$$\Delta T = \frac{\dot{m}_A}{\dot{m}_A + \dot{m}_P} \frac{1}{c_p} \sum_{j=1}^{K_g} \Delta h_{R,j} \Delta \xi_j \tag{14}$$

In Eq. 14 ($\dot{m}_A$) and ($\dot{m}_P$) denote the mass flow in the active and passive channel, respectively, and ($\Delta \xi$) denotes the conversion factor for each fuel (CO, H_2, CH_4). This methodology, although somewhat simplified, is a way to estimate the species and temperature profiles in the monolith. For the purpose of this investigation, this should be a sufficient approximation, considering that the reactions in the active channels are largely completed.

Homogeneous zone

The gas from the active and passive channels is assumed to mix instantaneously at the entrance to the homogeneous zone. If, for example, one-half of the channels are active, then it is assumed that for each species one-half of the exit mole fraction from the active channels is mixed with one-half of the exit mole fraction from the passive channels.The subsequent homogeneous zone after the monolith is modeled using SENKIN (Lutz et al., 1988), which is part of the CHEMKIN Collection (Kee et al., 2000). It is assumed that the homogeneous zone can be modeled with a plug-flow model, that is, mixing effects in the homogeneous zone after the monolith are negligible. Perfect mixing after the monolith may be a simplified hydrodynamic assumption, and the usability of a plug-flow model to model the homogeneous zone is further addressed in the Results and Discussion section of this article.

Table 1. Composition of Gasified Biomass (mol %)

Species	Typical Real Gasified Biomass	Synthetic Gas*	Synthetic Gas Mixed with Air ($\lambda = 2.5$)
N_2	41–50	44.9	69.8
O_2	0	0	15.3
H_2	9–14	10.0	2.7
CO	14–18	15.0	4.1
CO_2	11–20	14.0	3.8
CH_4	5–7	5.0	1.4
H_2O	10–12	11.0	3.0
NH_3	0.02–0.3	0.1	0.027

*Composition used in the calculations.

The equations solved in SENKIN are (adiabatic system with constant pressure):

Species continuity

$$\frac{dY_j}{dt} - \frac{\dot{\omega}_j W_j}{\rho} = 0 \qquad (j = 1, \ldots, K_g) \tag{15}$$

Thermal energy

$$c_p \frac{dT}{dt} + \frac{1}{\rho} \sum_{j=1}^{K_g} h_j \dot{\omega}_j W_j = 0 \tag{16}$$

The state expressed by Eq. 6 has to be added to the system.

Model fuel

The composition of biogas varies with the method of gasification and the composition of the raw biomass material. The composition of gasified biomass listed in Table 1 is, therefore, an attempt to summarize the distribution of the main components. The synthetic gas is used in all simulations, in order to simplify the numerical treatment. C_2-C_{12} hydrocarbons and trace components (that is, HCN, H_2S, and alkali components) were not included.

Chemical kinetic model

Both the gas-phase chemistry and the reactions on the catalyst surface were described in terms of detailed reaction mechanisms. The gas-phase chemistry is described with a chemical kinetic model for hydrocarbon–ammonia–nitric oxide interactions (Glarborg et al., 1998; Miller and Glarborg, 1999). This consists of 460 reactions among 66 species. In a hybrid catalytic combustor the thermal stress of the catalytic material is reduced. This means that Pt, which otherwise may not be the preferred active component for catalytic combustion of biomass, can be used. Consequently, the heterogeneous reactions in the active channels, which are assumed to take place on a polycrystalline Pt-surface with a site density of 2.71×10^{-9} moles/cm^2, were adopted from Deutschmann et al. (1996). This mechanism describes the catalytic ignition of CH_4, CO, and H_2 oxidation at atmospheric pressure. We have extrapolated the mechanism for at least a qualitative prediction of the behavior at elevated pressures. Pore diffusion effects are not accounted for. More catalyst washcoat would lead to a higher site density and a higher reaction rate.

To take into account that NH_3 is oxidized on Pt, we have added an NH_3 subset in this study (see Table 2). In the mechanism, Pt(s) denotes a free Pt site, X(s) an adsorbed species, and X a gas-phase species. The mechanism was constructed with the assumption that at higher temperatures the predominant product of ammonia oxidation on Pt is NO (for example, Cook, 1975). As the process is mass transfer limited, the details of the individual steps on the surface are less significant. The sticking coefficient for NH_3 was set to 0.1 in all calculations, and the presence of NH_3 did not significantly affect the oxidation of the other combustibles on the Pt surface.

Table 2. Reaction Mechanism for NH_3 Oxidation on Pt

	A^*	E_a^*
1. $NH_3 + 2\,Pt(s) \rightarrow NH_2(s) + H(s)$	0.1**	0
2. $NH_2(s) + Pt(s) \rightarrow NH(s) + H(s)$	3.7×10^{21}	20
3. $NH(s) + Pt(s) \rightarrow N(s) + H(s)$	3.7×10^{21}	20
4. $N(s) + O(s) \rightarrow NO(s) + Pt(s)$	3.7×10^{21}	20
5. $NO(s) \rightarrow NO + Pt(s)$	1.0×10^{13}	20

*Arrhenius parameters for the rate constants written in the form: $k_f = A \exp(-E_a/RT)$. The units of A are given in terms of moles, cubic centimeters, and seconds; E_a is in kJ·mol^{-1}.
**Sticking coefficient.

Results and Discussion

The advantage with our reactor concept is that only part of the fuel is catalytically converted in the monolith and thereby provides safe ignition of the low-heating-value gas. The use of passive channels in the monolith controls the temperature profile and avoids homogeneous ignition. After the monolith the unreacted gas from the passive channels are mixed with the partly reacted gas from the active channels. No reactants/reductants have to be added, as they already are part of the incoming fuel gas.

In the catalyst of a hybrid combustor fueled with natural gas, the homogeneous reactions play a minor role. However, in gasified biomass there is a considerable amount of H_2, which facilitates homogeneous ignition in the passive channels. Therefore, in order to avoid homogeneous ignition, the ratio of active to passive channels in the monolith has to be varied, depending on the stoichiometry in this region.

In the following we discuss two overall strategies to operate the hybrid catalytic combustor overall fuel-lean for maximum gas turbine efficiency and emitting low concentrations of CO, hydrocarbons, and NO_x. The first strategy is to work fuel-lean both in the monolith and in the subsequent homogeneous zone, and to use the SNCR reactions to reduce the formed NO_x in the active channels. The second strategy is to work fuel-rich in the monolith and then to add air downstream in the homogeneous zone. We thereby obtain a high-temperature reducing zone after the catalyst, where a reduction of NO may be favored.

Lean primary λ

First the reduction potential for a lean primary excess air ratio of 2.5 was estimated. This corresponds to the overall stoichiometry and results in the adiabatic temperature to the turbine without need for additional air. To avoid homogeneous ignition in the passive channels, the ratio of active to passive channels was 1:5 for the chosen value of λ.

Table 3. Estimated Temperature Profiles in the Monolith*

Axial Distance (cm)	Temp. Adiabatic Channel (K)	Temp. 1/5 Active Channels (K)
0	753	753.0
0.01	802	762.8
0.02	1,179	946.2
0.03	1,694	941.2
0.04	1,682	938.8
0.05	1,673	937.0
0.06	1,667	935.8
0.07	1,661	934.6
0.08	1,657	933.8
0.09	1,653	933.0
0.10	1,650	932.4
0.11	1,647	931.8
0.14	1,639	930.2
0.20	1,627	927.8
0.30	1,611	924.6
0.40	1,599	922.2
0.50	1,590	920.4
0.60	1,586	919.6
0.70	1,583	919.0
0.80	1,580	918.4
0.90	1,580	918.4
1.00	1,579	918.2
2.00	1,575	917.4
5.00	1,575	917.4

*Primary $\lambda = 2.5$; $T_{in} = 753\ K$; $u_{in} = 1$ m/s.

The predicted surface temperature profile in a monolith with 20% active channels under adiabatic conditions is shown in Table 3.

A contour plot of the temperature and selected gas-phase species concentrations in the active channels of a monolith with length 5.0 cm is shown in Figure 2. The length of the monolith was chosen to avoid significant conversion in the passive channels. The conversion is almost complete for CO, H_2, and NH_3, but only 35% for CH_4 as a result of the lower temperature rise compared to an adiabatic channel. The NO formed in the catalytic combustion of NH_3 is converted to NO_2 at the conditions studied. The elevated pressure facilitates the NO_2 formation; at atmospheric conditions the main product is NO. The estimated gas-phase composition after the monolith is shown in Table 4.

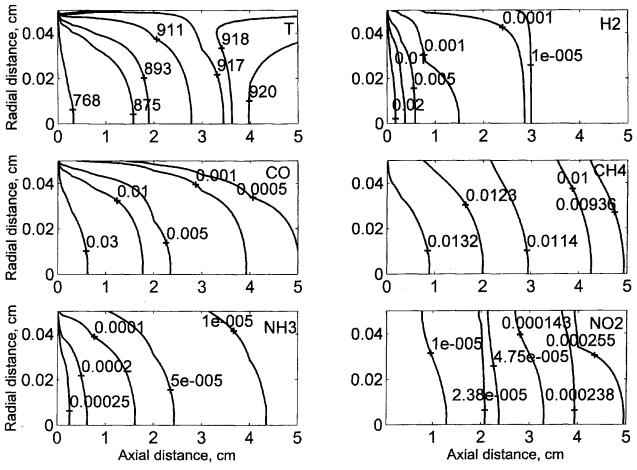

Figure 2. Contour of the temperature (K) and selected species (mole fractions) in the monolith channel.

$\lambda = 2.5$; $u_{in} = 1$ m/s; $T_{in} = 753$ K; length = 5 cm; active channels/passive channels = 1/5.

The NH_3 oxidation chemistry and the SNCR reactions are strongly dependent on the reaction temperature and composition. Without combustible components in the gas mixture, at below roughly 1,050 K, little or no reaction between NO and NH_3 takes place. As the temperature is increased, the following (simplified) reaction sequence becomes active

$$NH_3 + OH = NH_2 + H_2O \quad (17)$$

$$NH_2 + NO = N_2 + H + OH \quad (18a)$$

$$NH_2 + NO = N_2 + H_2O \quad (18b)$$

$$H + O_2 = O + OH \quad (19)$$

$$O + H_2O = 2OH \quad (20)$$

Since the key amine radical, NH_2, reacts almost solely with NO, a significant reduction in NO can be obtained. A further increase in temperature beyond an optimum value promotes oxidation of NH_i radicals to NO, resulting in an increase in NO. If combustibles like CO, H_2, and CH_4 are present in the gas mixture, the optimum temperature for the SNCR reactions is decreased. This can be attributed to the increased generation of chain carriers caused by the oxidation of these species, as shown for CO by Alzueta et al. (1997). The optimum temperature for the SNCR reactions is decreased with increased concentration of combustibles. However, when the combustible reactants are oxidized, the adiabatic temperature rise is significant, increasing the temperature above the window for the SNCR reactions. Instead of reacting with NO, the NH_3 is largely oxidized to NO, as seen in Figure 3. A parametric study indicates that the total reduction potential is below 6%. The conclusion is that the NH_3 content in the biogas cannot be used actively for NO reduction under these conditions due to the large fraction of combustibles in the biogas.

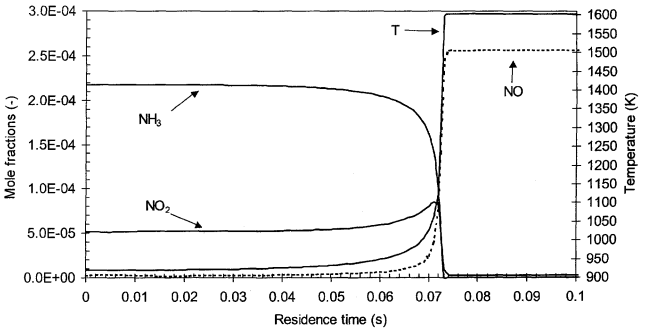

Figure 3. Profiles of temperature, NH_3, NO, and NO_2 as a function of residence time in the homogeneous zone after the monolith; the inlet composition is taken from Table 4.

Table 4. Estimated Composition (mole fractions) of the Gas at the Exit of the Monolith*

Species	Active Channels	Passive Channels	After Mixing
N_2	0.722318	0.697429	0.702407
O_2	0.113000	0.153000	0.145000
H_2	0.000000	0.027000	0.021600
CO	0.000197	0.040600	0.032519
CO_2	0.086100	0.038100	0.047700
CH_4	0.008810	0.013600	0.012642
H_2O	0.069300	0.030000	0.037860
NH_3	0.000004	0.000271	0.000218
NO_2	0.000260	0.000000	0.000052
NO	0.000011	0.000000	0.000002

*Primary $\lambda = 2.5$; $T_{in} = 753$ K; $u_{in} = 1$ m/s; length = 5 cm; active channels/passive channels = 1/5.

Rich primary λ

If the primary excess air ratio is decreased below stoichiometric to 0.8 the situation changes. The adiabatic temperature of the mixture is significantly increased, requiring a reduction of the ratio of active to passive channels in order to avoid homogeneous ignition in the passive channels. The predicted surface temperature profile in a monolith with adiabatic and 1/6 active channels is shown in Table 5. In Figure 4 a contour plot of temperature and selected gas-phase species in the monolith is shown. In principle it should be possible by trial and error to find a condition such that temperature rise and conversion become proportional according to Eq. 14. Here we have compared two surface temperature profiles: In the first case the temperature rises faster than the conversion of combustible species (length 1.5 cm), and in the second case it rises slower than the conversion (length 2.5 cm). As can be seen the final composition does not differ significantly for the two cases. The limiting reactant oxygen is consumed in both cases, but for different residence times.

The conversion in the active channels is almost complete for H_2 and NH_3, but only 60% for CO and 70% for CH_4 as a result of the rich conditions and the temperature profile in the monolith (see Table 6). Compared to the conditions just given with a lean primary stoichiometry, the conversion of methane has increased and no NO_2 is formed due to the air deficit.

The results from the subsequent homogeneous zone after mixing are shown in Figures 5–7. The temperature rises very

Table 5. Estimated Temperature Profile in the Monolith*

Axial Distance (cm)	Temp. Adiabatic Channel (K)	Temp. 1/6 Active Channels (K)
0	753.0	753.0
0.1	778.0	757.2
0.2	812.0	763.0
0.3	1,945.0	955.6
0.4	1,953.0	957.0
0.5	1,956.0	957.5
0.6	1,956.7	957.6
0.7	1,956.9	957.7
0.8	1,957.0	957.7
1.5	1,957.5	957.8

*Primary $\lambda = 0.8$; $T_{in} = 753$ K: $u_{in} = 1$ m/s.

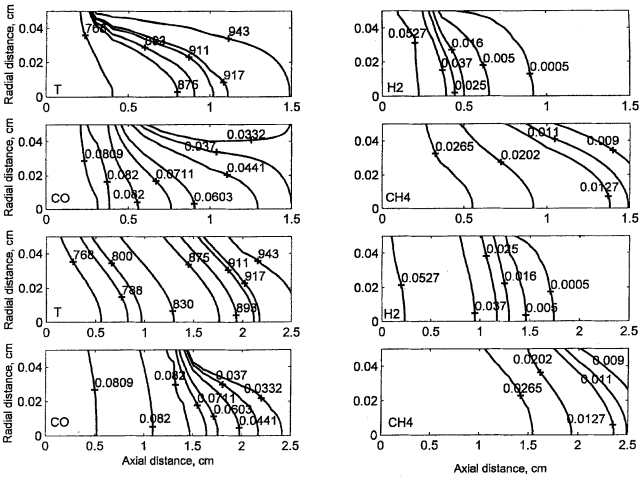

Figure 4. Contour of the temperature (K) and selected species (mole fractions) in the monolith channel for two different wall temperature profiles.

$\lambda = 0.8$; $u_{in} = 1$ m/s; $T_{in} = 753$ K; active channels/passive channels = 1/6.

rapidly in the main reaction zone where all methane and ammonia are consumed, and then it has an almost constant value. First a significant amount of NO is formed from oxidation of NH_3 before all oxygen is consumed. The NO is subsequently reduced to N_2, and the reduction is better for longer residence times.

A reaction path analysis in the high-temperature regime (> 1900 K) reveals that there are two major channels for consumption of NO in the absence of oxygen

Channel I

$$NO + H \rightarrow N + OH \tag{21}$$

$$N + NO \rightarrow N_2 + O \tag{22}$$

Channel II

$$NO + H + M \rightarrow HNO + M \tag{23}$$

$$HNO + H \rightarrow NH + OH \tag{24}$$

Table 6. Estimated Composition (mole fractions) of the Gas at the Exit of the Monolith*

Species	Active Channels	Passive Channels	After Mixing
N_2	0.638839	0.607006	0.612418
O_2	0.006020	0.096400	0.081035
H_2	0.000004	0.053100	0.044074
CO	0.034000	0.080200	0.072346
CO_2	0.152000	0.075900	0.088837
CH_4	0.007600	0.026900	0.023619
H_2O	0.161000	0.059900	0.077087
NH_3	0.000012	0.000537	0.000448
NO	0.000525	0.000000	0.000089
C_2H_6	0.000000	0.000002	0.000002
H_2O_2	0.000000	0.000024	0.000020
CH_2O	0.000000	0.000031	0.000026

*Primary $\lambda = 0.8$; $T_{in} = 753$ K; $u_{in} = 1$ m/s; length = 1.5 cm; active channels/passive channels = 1/6.

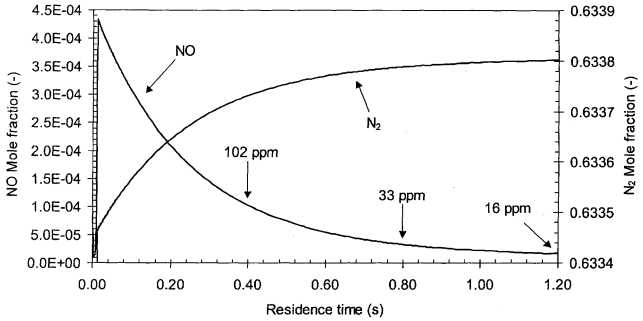

Figure 5. Profiles of NO and N_2 as a function of residence time in the homogeneous zone after the monolith.

The inlet composition is taken from Table 6. A significant amount of NO is formed from oxidation of NH_3 before all oxygen is consumed. The NO is subsequently reduced to N_2.

$$NH + NO \rightarrow N_2O + H \quad (25)$$

$$N_2O + M \rightarrow N_2 + O + M \quad (26)$$

The reduction of NO is facilitated by the presence of the unburned fuel components CO and H_2, as they produce the H radical needed in the two channels

$$CO + OH \rightarrow CO_2 + H \quad (27)$$

$$H_2 + OH \rightarrow H_2O + H \quad (28)$$

The participation of CO and H_2 is shown in Figure 6, where their concentration declines slowly even after all the oxygen is consumed. The reduction of NO by CO and H_2 was also shown in a laboratory study (Glarborg et al., 2000).

To burn out the remaining CO and H_2, additional air is added downstream of the rich primary zone (see Table 7). The final NO concentration depends on the residence time in the reducing zone; under the present conditions it is 13 ppm, that is, a reduction efficiency of 95% (see Figure 8).

If the inlet velocity is increased to 7 m/s, the ignition distance in the monolith is increased from 0.3 cm to 1.7 cm. But

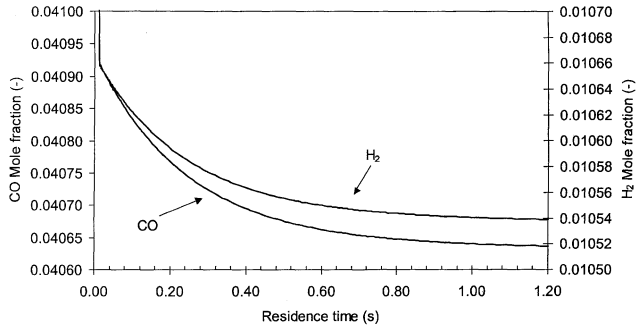

Figure 6. Profiles of CO and H_2 as a function of residence time in the homogeneous zone after the monolith.

The inlet composition is taken from Table 6. Under the oxygen deficit conditions prevailing after the reaction zone, CO and H_2 help to reduce the formed NO by forming H radicals.

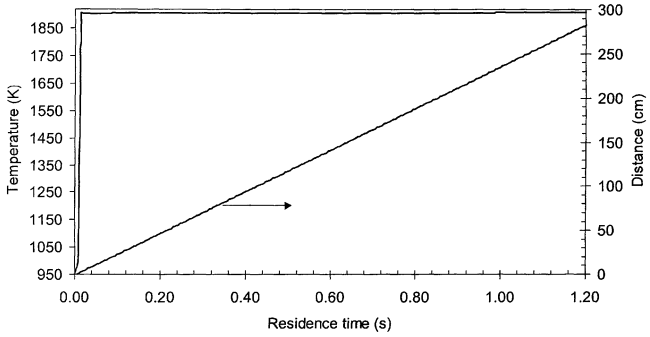

Figure 7. Profiles of temperature and distance as a function of residence time in the homogeneous zone after the monolith: the inlet composition is taken from Table 6.

the same composition after mixing can be achieved, indicating the same reduction potential in the homogeneous zone. Reducing the inlet temperature to 673 K also increased the ignition distance in the monolith significantly, from 0.3 cm to 12.3 cm, but the NO_x reduction potential in the homogeneous zone was not changed significantly. A recuperate reactor to generate higher inlet temperatures would therefore decrease the precious-metal cost with the same reduction efficiency.

The combustion chamber designs studied here have been simulated for realistic conditions regarding temperature and pressure for gas turbines. A primary λ of 0.8 gave a NO_x reduction efficiency of 95%. However, even higher reduction efficiencies may be achieved if an optimum primary λ can be found that is rich enough to keep NO low and lean enough to avoid excessive HCN formation. The temperature in the homogeneous zone should be high enough for fast NO reduction, but low enough to avoid thermal NO_x production. The configuration of active/passive channels in the monolith has to be adjusted accordingly to avoid homogeneous ignition in the passive channels of the monolith.

The final parameter to consider is that a high residence time is needed in the homogeneous combustion section for the NO_x reduction to reach the desirable extent. This may be possible, using a combustion chamber of a tubular design for which residence times of several seconds are possible at least in principle (Perry et al., 1999).

Obviously, the mixing region after the monolith is critical, and here a plug-flow model may not be able to catch all the details of the mixing process. We performed calculations with

Table 7. Estimated Composition into the Secondary Zone*

Species	Before Mixing	After Air Addition
N_2	0.633855	0.704562
O_2	0	0.095089
CO	0.040636	0.022236
H_2	0.010539	0.005767
H_2O	0.164386	0.089950
CO_2	0.150567	0.082388
NO	0.000016	0.000009

*Air at 753 K is added downstream of the primary zone to burn out the remaining CO and H_2. The overall λ after mixing is 2.5 and the residence time is 1.2 s.

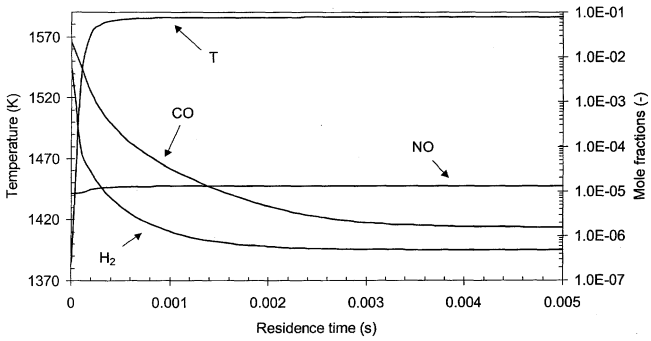

Figure 8. Profiles of temperature, CO, H_2, and NO after air-addition.

Inlet composition is according to Table 7. Close to 13 ppm NO remains after combustion, which means an overall reduction of 95% for a primary λ of 0.8.

OPPDIF (Lutz et al., 1996; Kee et al., 2000) and the composition in Table 6 to study the influence of mixing. A diffusion flame was established in the mixing layer at the outlet of the active and passive channels. However, the concentration of NO predicted by OPPDIF was not higher than the concentration predicted with the plug-flow model shown in Figure 5.

In the NO_x reduction zone ($T > 1{,}900$ K) the Reynolds number is around 1,000, clearly in the laminar flow regime. At higher inlet velocities the Reynolds number will be in the turbulent regime where plug-flow models usually are valid (Raja et al., 2000). We performed additional calculations with CRESLAF and PREMIX to compare the plug-flow model with models that include diffusion (Kee et al., 1985; Kee et al., 2000). These calculations predicted a similar or even a faster NO reduction than the plug-flow model.

The additional calculations for both the mixing zone (temperature from 953 K to 1900 K) and subsequent NO_x reduction zone show that a plug-flow model, with its assumptions regarding mixing, is able to reasonably predict the behavior. This implies that the chemical kinetics is of more importance than the flow model used.

Conclusions

A design concept for a catalytic combustion chamber design, with the ability to reduce the fuel-NO_x at conditions relevant to catalytic combustion of gasified biomass, has been proposed. This design consists of a monolith with passive and active channels, where only part of the fuel is combusted catalytically in the active channels. The completion of the reactions is carried out in the subsequent homogeneous zone.

The primary fuel–air ratio is found to be the most important parameter for the NO_x reduction potential. A critical factor in the design is the ratio between active and passive channels. When a lean primary stoichiometry is used, no favorable conditions are established for the selective noncatalytic reactions (SNCR) due to the large fraction of combustibles in the biogas. When they are oxidized, the adiabatic temperature rise is significant, increasing the temperature above the window for the SNCR reactions. However, if the air supply to the monolith is staged rich-lean, a 95% reduction of NO is possible.

The NO reduction is facilitated by the presence of the fuel components CO and H_2, as they produce the H radicals needed in NO reduction reactions.

A plug-flow model, with its assumptions regarding mixing, is able to reasonably predict the behavior in the homogeneous zone after the monolith.

Acknowledgments

The work is supported financially by the Swedish Foundation for Strategic Research, The Center for Combustion Science and Technology, and the Swedish Energy Agency. One of the authors (J.A.) is grateful for the stay at the CHEC (Combustion and Harmful Emission Control) Research Center at DTU during the spring of 2002. Finally, the authors thank Professor Bob Kee at Colorado School of Mines for his valuable comments.

Notation

c_p = specific heat, $J \cdot kg^{-1} \cdot K^{-1}$
$D_{j,m}$ = mixture–average diffusion coefficient of species j in mixture, $cm^2 \cdot s^{-1}$
D_j^T = thermal diffusion coeffcient, $g \cdot cm^{-1} \cdot s^{-1}$
h_j = specific enthalpy of species j, $J \cdot kg^{-1}$
k = thermal conductivity, $W \cdot cm^{-1} \cdot K^{-1}$
K_g = number of gas-phase species
K_s = number of surface species
$\dot{m}_A$ = mass flow in active channel, $g \cdot s^{-1}$
$\dot{m}_P$ = mass flow in passive channel, $g \cdot s^{-1}$
N_s = number of surface reactions
p = pressure, Pa
r = cross-flow coordinate, cm
r_i^s = rate of ith surface reaction, $mol \cdot cm^{-2} \cdot s^{-1}$
R = universal gas constant, $J \cdot mol^{-1} \cdot K^{-1}$
$\dot{s}_j$ = chemical production rate of species j by surface reaction, $mol \cdot cm^{-2} \cdot s^{-1}$
u = axial velocity, $cm \cdot s^{-1}$
T = temperature, K
v = fluid velocity in the radial direction, $cm \cdot s^{-1}$
$J_{j,r}$ = mass flux in radial direction, $g \cdot cm^{-2} \cdot s^{-1}$
W_j = molecular weight of species j, mol^{-1}
$\overline{W}$ = mean molecular weight of the mixture, mol^{-1}
X_j = mole fraction of species j
Y_j = mass fraction of gas-phase species j
z = axial coordinate, cm
Z_j = site fraction of species j

Greek letters

$\Delta h_{R,j}$ = heat of reaction for fuel j, $J \cdot kg^{-1}$
$\Delta \xi_j$ = conversion factor for fuel j
λ = excess air ratio
μ = viscosity, $g \cdot cm^{-1} \cdot s^{-1}$
ρ = mass density, $g \cdot cm^{-3}$
ν_{ij} = stoichiometric coefficient of jth species in ith reaction
v_{st} = Stefan velocity, $cm \cdot s^{-1}$
$\dot{\omega}_j$ = chemical production rate of species j by gas-phase reaction, $mol \cdot cm^{-3} \cdot s^{-1}$

Superscripts and subscripts

g = gas
i = reaction
j = species
s = surface

Literature Cited

Alzueta, M. U., H. Røjel, P. G. Kristensen, P. Glarborg, and K. Dam-Johansen, "Laboratory Study of the CO/NH_3/NO/O_2 System: Implications for Hybrid Reburn/SNCR Strategies," *Energy Fuels,* **11**, 716 (1997).

Burch, R., and B. W. L. Southward, "A Novel Application of Trapping Catalysts for the Selective Low-Temperature Oxidation of NH_3 to N_2 in Simulated Biogas," *J. Catal.*, **195**, 217 (2000).

Burch, R., and B. W. L. Southward, "The Nature of the Active Metal Surface of Catalysts for the Clean Combustion of Biogas Containing Ammonia," *J. Catal.*, **198**, 286 (2001).
Clark, W. D., B. A. Folsom, W. R. Seeker, and C. W. Courtney, "Bench Scale Testing of Low-NO_x LBG Combustors," *J. Eng. Power*, **104**, 120 (1982).
Coltrin, M. E., H. K. Moffat, R. J. Kee, and F. M. Rupley, "CRESLAF (Version 4.0): A Fortran Program for Modeling Laminar, Chemically Reacting, Boundary-Layer Flow in Cylindrical or Planar Channels," Sandia National Laboratories Rep. SAND93-0478, Albuquerque, NM (1993).
Cook, G., *Survey of Modern Industrial Chemistry*, Ann Arbor Science Publishers, Ann Arbor, MI, p. 235 (1975).
Dalla Betta, R. A., J. C. Schlatter, D. K. Yee, D. G. Loffler, T. Shoji, "Catalytic Combustion Technology to Achieve Ultra Low NO_x Emissions: Catalyst Design and Performance Characteristics," *Catal. Today*, **26**, 329 (1995).
Deutschmann, O., R. Schmidt, F. Behrendt, and J. Warnatz, "Numerical Modeling of Catalytic Ignition," *Proc. Combust. Inst.*, **26**, 1747 (1996).
Forzatti, P., and G. Groppi, "Catalytic Combustion for the Production of Energy," *Catal. Today*, **54**, 165 (1999).
Glarborg, P., M. U. Alzueta, K. Dam-Johansen, and J. A. Miller, "Kinetic Modeling of Hydrocarbon/Nitric Oxide Interactions in a Flow Reactor," *Combust. Flame*, **115**, 1 (1998).
Glarborg, P., P. G. Kristensen, K. Dam-Johansen, M. U. Alzueta, A. Millera, and R. Bilbao, "Nitric Oxide Reduction by Non-Hydrocarbon Fuels. Implications for Reburning with Gasification Gases," *Energy Fuels*, **14**, 828 (2000).
Groppi, G., A. Belloni, E. Tronconi, and P. Forzatti, "Analysis of Multidimensional Models of Monolith Catalysts for Hybrid Combustors," *AIChE J.*, **41**, 2250 (1995).
Groppi, G., E. Tronconi, M. Berg, and P. Forzatti, "Development and Application of Mathematical Models of Pilot-Scale Catalytic Combustors Fueled by Gasified Biomasses," *Ind. Eng. Chem. Res.*, **39**, 4106 (2000).
Johansson, E. M., *Catalytic Combustion of Gasified Biomass for Gas Turbine Applications*, PhD Thesis, Royal Institute of Technology, Stockholm, Sweden (1998).
Johansson, E. M., D. Papadias, P. G. Thevenin, A. G. Ersson, R. Gabrielsson, P. G. Menon, P. H. Björnbom, and S. G. Järås, "Catalytic Combustion for Gas Turbine Applications," *Catalysis*, Vol. 14, Royal Society of Chemistry, Cambridge, p. 183 (1999).
Kee, R. J., J. F. Grcar, M. D. Smooke, and J. A. Miller, "A Fortran Program for Modeling Steady Laminar One-Dimensional Premixed Flames," Sandia National Laboratories Rep. SAND85-8240, Livermore, CA (1985).
Kee, R. J., F. M. Rupley, J. A. Miller, M. E. Coltrin, J. F. Grcar, E. Meeks, H. K. Moffat, A. E. Lutz, G. Dixon-Lewis, M. D. Smooke, J. Warnatz, G. H. Evans, R. S. Larson, R. E. Mitchell, L. R. Petzold, W. C Reynolds, M. Caracotsios, P. Stewart, P. Glarborg, C. Wang, and O. Adigun, *Chemkin Collection*, Release 3.6, Reaction Design, Inc., San Diego, CA (2000).
Kee, R. J., M. E. Coltrin, and P. Glarborg, *Chemically Reacting Flow — Theory and Practice*, Wiley, New York, p. 318 (2003).
Lietti, L., C. Ramella, G. Groppi, and P. Forzatti, "Oxidation of NH_3 and NO_x Formation During the Catalytic Combustion of Gasified Biomasses Fuels over Mn-Hexaaluminate and Alumina-Supported Pd Catalysts," *Appl. Catal. B*, **21**, 89 (1999).
Lutz, A. E., R. J. Kee, and J. A. Miller, "SENKIN: A Fortran Program for Predicting Homogeneous Gas Phase Chemical Kinetics with Sensitivity Analysis," Sandia National Laboratories Rep. 87-8248, Livermore, CA (1988).
Lutz, A. E., R. J. Kee, J. F. Grcar, and F. M. Rupley, "OPPDIF: A Fortran Program for Computing Opposed-Flow Diffusion Flames," Sandia National Laboratories, Rep. 96-8243, Livermore, CA (1996).
Miller, J. A., and P. Glarborg, "Modeling the Thermal $DeNO_x$ Process: Closing in on a Final Solution," *Int. J. Chem. Kinet.*, **31**, 757 (1999).
Perry, R. H., D. W. Green, and J. O. Maloney, eds., "Gas Turbines," *Perry's Chemical Engineers' Handbook*, 7th ed., McGraw-Hill, New York, p. 29 (1997).
Raja, L. L., R. J. Kee, O. Deutschmann, J. Warnatz, and L. D. Schmidt, "A Critical Evaluation of Navier-Stokes, Boundary-Layer, and Plug-Flow Models of the Flow and Chemistry in a Catalytic-Combustion Monolith," *Catal. Today*, **59**, 47 (2000).

Manuscript received June 28, 2002, and revision received Feb. 4, 2003.